

## Design and analysis of an FUV spectrograph for a small satellite

Rahul Munshi,<sup>1</sup> B. R. Prasad<sup>2</sup> and Jayant Murthy<sup>2\*</sup>

<sup>1</sup>*Dept. of Physics and Meteorology, Indian Institute of Technology, Kharagpur 721302, India*

<sup>2</sup>*Indian Institute of Astrophysics, Bangalore 560034, India*

Received 1 July 2008; accepted 7 May 2009

**Abstract.** The Halo Ultraviolet Explorer (HUE) is a payload aimed at studying the diffuse far ultraviolet sky over a bandpass of 800 – 1200 Å. The novel features of HUE include a large effective collecting area (254 cm<sup>2</sup>) and fast ( $f/2.2$ ) optics in a compact design optimized for a standard small satellite bus. We have investigated two different models, each with an 18 cm off-axis parabolic primary mirror, but one with an additional folding mirror to decrease the total length of the spectrograph. The spectrograph slit is dumbbell shaped maximizing the spectral resolution in the centre of the slit while increasing the sensitivity to diffuse sources at the edges. The primary scientific goal of the mission is to investigate the distribution of O VI in the Galactic halo. This line is a sensitive indicator of the hot gas in the interstellar medium and is critical in understanding the dynamics and energetics of the Galaxy.

*Keywords :* Galaxy, interstellar medium, UV instrumentation

### 1. Introduction

There are several contributors of astrophysical importance to the far ultraviolet (FUV) — that part of the spectrum between 900 and 1200 Å (the Lyman limit to the Ly $\alpha$  line of hydrogen). This spectral range includes tracers of both the hot phase of the interstellar medium (ISM) in the 977 Å line of C III and the 1032/1038 Å doublet of OVI and of the cold phase in the Lyman and Werner bands of molecular hydrogen. Continuum emission from dust scattering pervades the entire spectral range and provides a measure

---

\*email: murthy@iiap.res.in

**Table 1.** Spacecraft bus specifications.

Box dimensions (L × W × H)	1.7 m × 1m × 0.35 m
Weight	120 kg

of the reprocessing of starlight in our Galaxy and, by extension, in other galaxies as well. Although the importance of this spectral range and of observations of the diffuse sky have long been recognized, there have been technical difficulties in realizing the instrument over and above the need for space-based instrumentation (Murthy 2009).

Very few spacecrafts have observed the FUV sky and none have been optimized for the diffuse radiation field. The two major programs have been observations with the two Voyager spacecrafts (Murthy et al. 1999) and with the Far Ultraviolet Spectroscopic Explorer (Murthy & Sahnou 2004) but neither were designed to survey the diffuse FUV sky, particularly the hot gas which is our primary science objective. We are now designing a low cost, easy to realize spectrograph optimized for largescale surveys of the sky in this spectral region and, in this work, describe the optical design of such an instrument.

## 2. Requirements and design philosophy

Our science objective is to study the 300 Å range between the Lyman limit (912 Å) and Ly $\alpha$  (1216 Å) with a particular focus on separating the OVI doublet (1032/1038 Å) from the geocoronal Ly $\beta$  line at 1026 Å. This necessarily implies that we must use a spectrograph with a resolution of better than 6 Å at 1026 Å. As we want to use easily realizable components, we have baselined a 40 mm diameter wedge-and-strip detector with 100  $\mu$ m spatial resolution implying a spread on the focal plane of about 0.75 Å per 100  $\mu$ m resolution element. The slit width is set by a compromise between high spectral resolution, which demands a narrow slit, and high sensitivity to diffuse sources, which requires a large aperture. We have therefore adopted a dumb-bell shaped slit which gives a resolution sufficient to separate the different components of the diffuse radiation field in the slit centre but with much higher sensitivity at the edges.

The optical system has been designed as per a standard small satellite bus (Table 1) which is compatible with a large range of potential satellites ranging from those in low Earth orbit to geosynchronous satellites and may be easily modified as per specific requirements. There are very few materials which either reflect or transmit in the FUV and we have minimized the number of optical elements with no transmission optics. The entire instrument has been designed such that there will be no manufacturing or procurement issues.

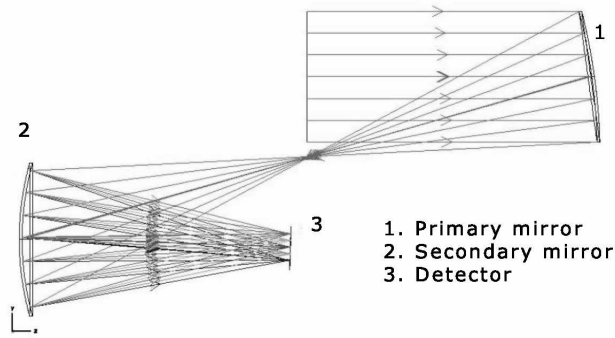


**Figure 1.** Model I: A 2-bounce system with a parabolic mirror (1) reflecting light off a toroidal grating (2) to a detector (3).

### 3. Optical design

Our basic optical design (Model I) is a simple two-bounce system, 800 mm long, (Fig. 1) with plane parallel wavefronts entering through a 180 mm diameter aperture stop. These are focused by an off-axis paraboloid onto a holographically ruled toroidal grating

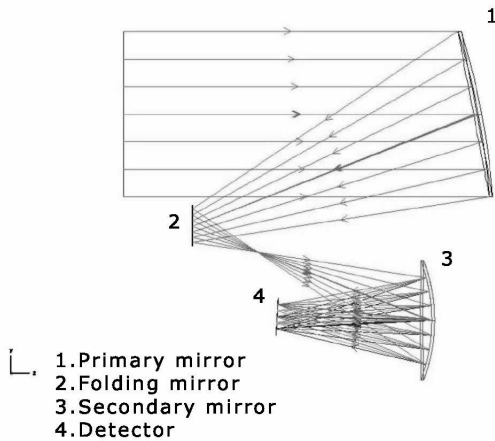


**Figure 2.** Model II: Same as Fig. 1 but with an additional folding mirror (2).

**Table 2.** Comparison between the two models.

Parameters	Model I	Model II
Primary mirror type	Off-axis paraboloid	Off-axis paraboloid
Effective surface area	254 cm <sup>2</sup>	254 cm <sup>2</sup>
Decentricity	110 mm	100 mm
Folding mirror	no	Yes (Plane mirror)
Reflecting surfaces	1	2
Spectral resolution	4.91 Å @ 1026 Å	5.08 Å @ 1026 Å
Slit to grating	390 mm	260 mm
Grating constant	2400 lines/mm	3900 lines/mm
Grating shape	Circular (220 mm dia.)	Circular (130 mm dia.)
Plate scale	426.2 arcseconds/mm	721.2 arcseconds/mm
Plate scale in spectral direction	10 Å/mm	10 Å/mm
Rad. of curvature	396 mm	189 mm
Rad. of rotation	382 mm	177.5 mm
diffraction order	1	1
Surface coating	SiC	SiC
Reflectivity at 1000 Å	0.4	0.4
Index of refraction at 912 Å	0.632 + 1.173 i	
Index of refraction at 1216 Å	0.97 + 1.640 i	

and then onto a detector at the focal plane. This configuration minimizes the number of reflections and thus maximizes the efficiency but is not as compact as Model II where we shrink the total length to 400 mm by adding a folding mirror (Fig. 2). The extra bounce cuts the efficiency by about a factor of 3 as our baseline mirror material (SiC) has a reflectance of about 40% at this wavelength. The physical characteristics of both models are given in Table 2.

The primary off-axis parabolic mirror has a circular aperture of diameter 180 mm in a plane parallel to the stop. It has no tilt and its aperture center is 110 mm and 100 mm above the axis of the paraboloid in Models I and II respectively. Being parabolic, the surface conic constant is fixed at -1. Operating at  $f/2.2$ , this mirror has a radius of curvature 792 mm in both models. It has a SiC coating of the desired thickness with a reflectivity of about 40% in this wavelength region.

The rays enter the spectrograph through a dumb-bell shaped slit placed at the primary (secondary) focus in Model I (Model II) before the grating. The narrow portion of the slit covers the central  $1.25^\circ$  of the field and has a width of 0.31 mm (corresponding to  $2.7'$ ) for a spectral resolution of 3.1 Å. The outer portion of the slit, where the image quality is poorer, has a width of 1.75 mm (corresponding to  $15'$ ) for a spectral resolution of 17.5 Å for diffuse sources with an increase of a factor of 6 in the sensitivity. Of course,

the spectral resolution and sensitivity are unchanged for point sources. The spectrograph grating in Model I has a grating constant of 2400 lines/mm and lies on a plane passing through the center of curvature of the primary mirror at a distance of 792 mm from the center of curvature. In order to avoid vignetting over the  $1.25^\circ$  field of view, the grating surface is circular with a diameter of 210 mm. Correspondingly, the grating center in Model II lies at a horizontal distance of 260 mm from the folding mirror center while the grating itself is circular with a diameter of 130 mm and 3900 lines/mm.

Coma is inherent in an off-axis paraboloid mirror and is worsened as the rays become more off-axis and the optics faster. We have minimized the aberrations by using a toroidal grating with the two perpendicular foci of the grating surface chosen to minimize the root mean square (r.m.s.) radii of the spots at the focal plane. We have also minimized the angle of incidence  $\alpha$  at the grating to  $16.1^\circ$  and  $31^\circ$  in Models I and II, respectively.

We plan to rule the reflection grating holographically onto a toroidal blank. Toroidal surfaces are described by defining a curve in the Y-Z plane, and then rotating this curve about an axis parallel to the Y axis and intersecting the Z axis. The curve defining the surface in Y-Z plane is given by

$$z = \frac{cy^2}{1 + \sqrt{1 - (1+k)c^2y^2}} \quad (1)$$

where  $c$  is the curvature and  $k$  is the conic constant. For  $k=0$  eqn. (1) reduces to

$$y^2 + \left(z - \frac{1}{c}\right)^2 = \frac{1}{c^2}. \quad (2)$$

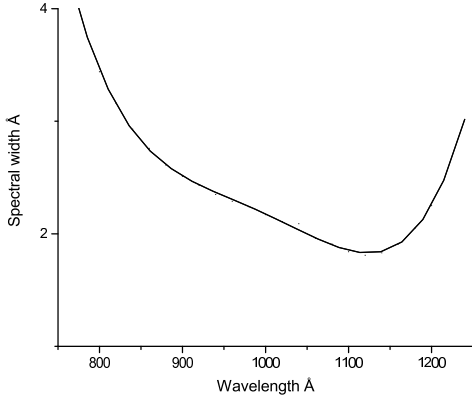
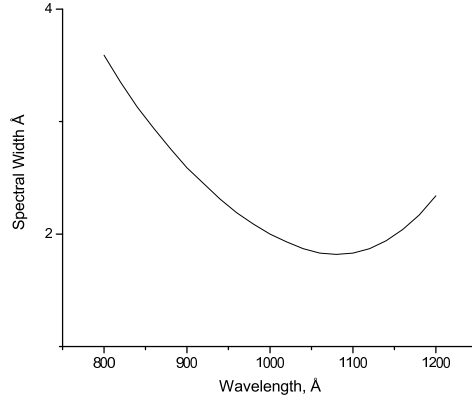
The radius of curvature ( $\frac{1}{c}$ ) is 396 mm in Model I and 189 mm in Model II, both operating at  $f/2.2$ . This curve is then rotated with a radius of rotation (R) being 382 mm in Model I and 177.5 mm in Model II. The radius of rotation and the radius of curvature are chosen such that the astigmatic foci match at the focal plane for the waveband of our interest. Such gratings have been holographically ruled for the Far Ultraviolet Spectroscopic Explorer (FUSE) mission with more than 5000 lines/mm by Jobin-Yvon (Wilkinson et al. 1998).

#### 4. Optical analysis

The spectrograph slit is a dumbbell shape with a  $3 \text{ \AA}$  projection of the slit on the focal plane. The net resolution is obtained by adding the blur circle radius to the projection of the slit to the focal plane. So for Model I, the net resolution varies from  $5 \text{ \AA}$  at  $1000 \text{ \AA}$  to  $6.58 \text{ \AA}$  at  $800 \text{ \AA}$  and  $5.18 \text{ \AA}$  at  $1200 \text{ \AA}$ . Similarly for Model II, the net resolution varies from  $5.17 \text{ \AA}$  at  $1000 \text{ \AA}$  to  $6.4 \text{ \AA}$  at  $800 \text{ \AA}$  and  $5.67 \text{ \AA}$  at  $1200 \text{ \AA}$ . These are tabulated in Table 3, along with the corresponding spectral width and the angular spread for zero angled fields. The spectral resolution at the detector is obtained by dividing the rms radius with focal plane scale as plotted for Model I in Fig. 3 and for Model II in Fig. 4.

**Table 3.** Blur circle radius for model I and model II.

Wavelength (Å)	RMS rad. ( $\mu\text{m}$ )	Model I		RMS rad. ( $\mu\text{m}$ )	Model II	
		angular width (arcmin)	spectral width (Å)		angular width (arcmin)	spectral width (Å)
800	358	3.34	3.58	258	5.2	3.44
900	260	2.42	2.6	188	3.85	2.5
1000	200	1.86	2	162.75	3.34	2.17
1100	170	1.88	1.7	138	2.82	1.84
1200	218	2.34	2.18	200.7	3.48	2.67

**Figure 3.** Model I, spectral resolution.**Figure 4.** Model II, spectral resolution.

The rms radius for a 1026 Å spot with a  $-0.625^\circ$  field angle is  $136 \mu\text{m}$  for Model I giving a spectral width of  $1.36 \text{ \AA}$ . The same spot for the  $0.625^\circ$  field is  $310 \mu\text{m}$  subtending a spectral width of  $3.1 \text{ \AA}$ . In Model II, the 1026 Å spot for field angle  $0.625^\circ$  has an rms radius of  $204.7 \mu\text{m}$  and hence a spectral width of  $2.733 \text{ \AA}$ . For  $-0.625^\circ$  field angle, the same spot rms radius is  $327 \mu\text{m}$  for an effective width of  $4.36 \text{ \AA}$ . The Huygens' diffraction encircled energy diagram shows the percentage of total energy enclosed as a function of distance from the image centroid at the image plane and are plotted for each model in Figs 5 and 6. The diffraction point spread function has been calculated using the direct integration of Huygens' wavelets methods with a sampling density of  $64 \times 64$ .

Spot diagrams for the two models are shown in Figs 7 and 8, respectively, for several wavelengths and for normal incidence and off-axis rays at  $\pm 0.625^\circ$ . We have optimized the design to minimize the spot size over the entire field of view of  $1.25^\circ$  and have found that the performance meets our required spectral resolution.

## 5. Tolerancing

Tolerance analysis determines the maximum change in the optical parameters that can still meet the performance requirements. We have performed a sensitivity analysis on each component independently with rms spot radius with reference to the centroid. This allows one to identify the worst offenders; i.e., those which had the greatest impact on the image quality. We could compensate to some extent by changing the radius of rotation of the grating surface, tilt of detector plane and grating detector distance and optimized them using a damped least square optimization algorithm. The estimated change in the image quality for each of the extreme values of the tolerances could then be computed by the root of the sum of the square (r.s.s) estimates where the difference is given by

$$\Delta = S(P - N)\sqrt{|P^2 - N^2|} \quad (3)$$

where,  $S(x)=1$  for all positive  $x$  and  $-1$  otherwise. Here  $P$  is the perturbed criterion and  $N$  is the nominal criterion. The total change is then computed by summing over all tolerances of the averaged squared values. i.e.

$$C^2 = \sum_i \frac{\Delta_{i,min}^2 + \Delta_{i,max}^2}{2} \quad (4)$$

Using r.s.s. for finding the final performance we get

$$F = \sqrt{N^2 + C^2} \quad (5)$$

where  $N$  is the nominal value and  $C$  is the change computed earlier. The tolerance data is estimated with 20 cycles of Monte-Carlo simulation giving an accurate appraisal of

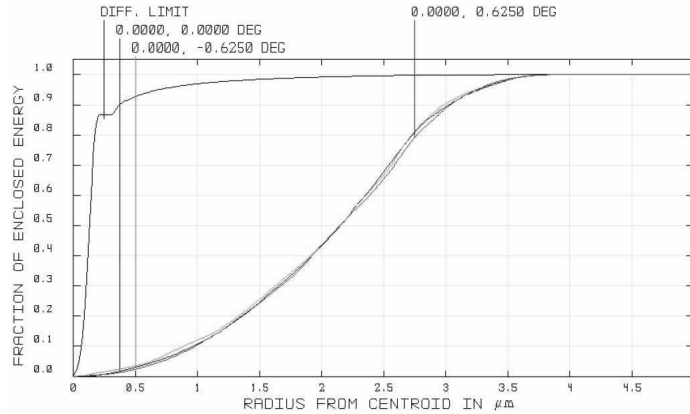


**Figure 5.** Model I, encircled energy diagram of the rays at  $\pm 0.625^\circ$  and  $0^\circ$  to the aperture.

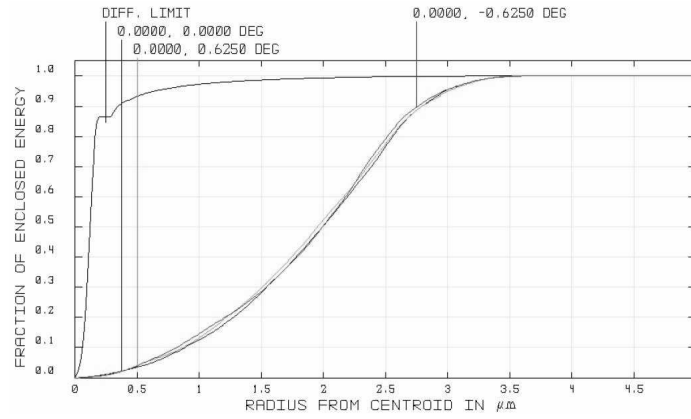


Figure 6. Model II, encircled energy diagram of the rays at  $\pm 0.625^\circ$  and  $0^\circ$  to the aperture.

the probability of success of the adopted tolerances. It estimates the performance of the system considering all the tolerances simultaneously. For each cycle, random parameters

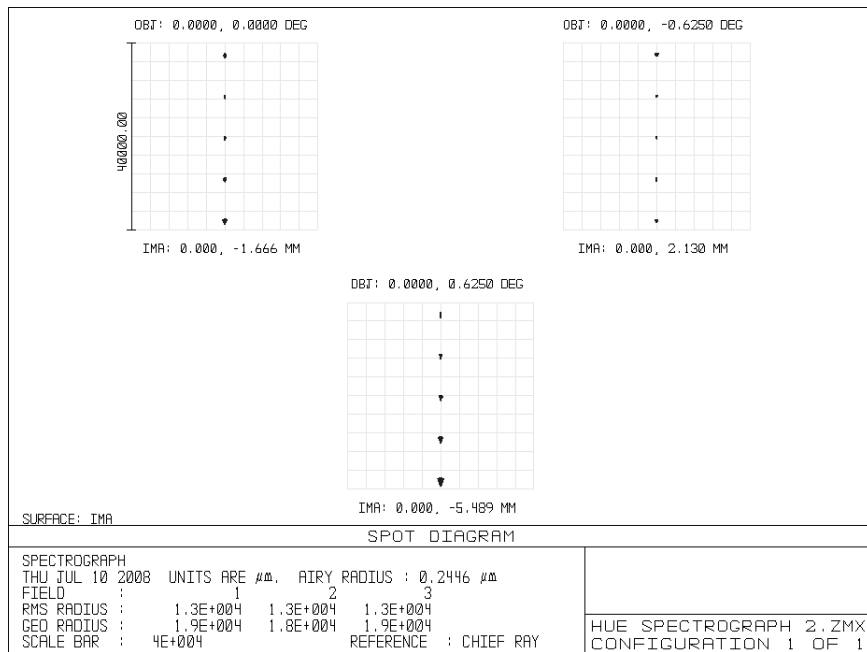
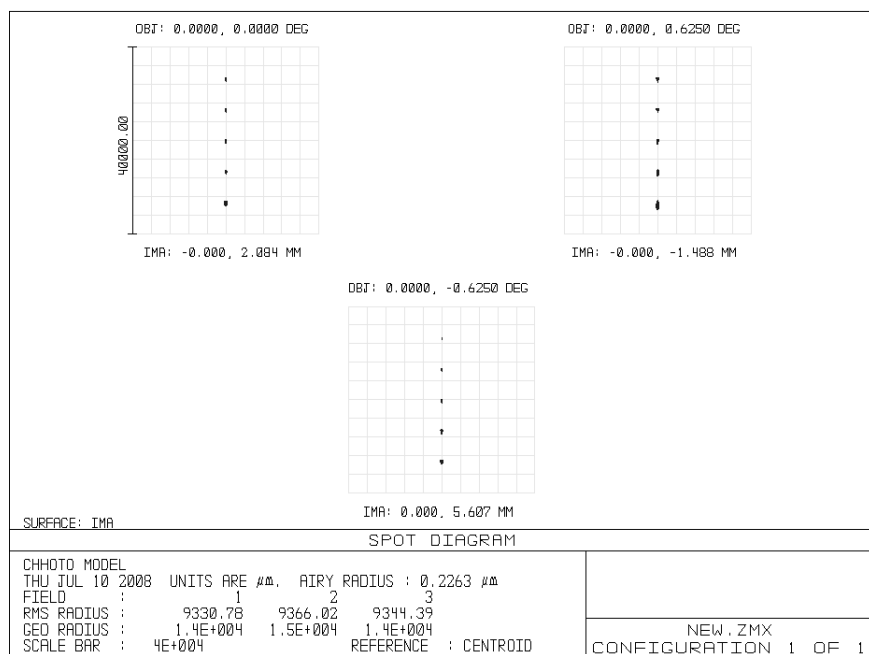


Figure 7. RMS spot diagram Model I.



**Figure 8.** RMS spot diagram Model II.

are set using a parabolic distribution which is given by

$$p(x) = \left(\frac{3x^2}{2\Delta^3}\right), -\Delta < x < \Delta \quad (6)$$

where  $x$  is a randomly selected value measured as an offset from the midpoint between the two extreme tolerances and  $\Delta$  is one half of the difference between the maximum and minimum tolerance values. As  $p(x)$  varies as the square of  $x$ , the distribution is clearly parabolic. This distribution yields the selected values that are more likely to be at the extreme ends of the tolerance range.

The tolerances listed here (Tables 4 and 5) are within the standard limits and the criterion is checked to be within the limits of desired optical performance. The limits of decenter, tilt and conic constant are purely the result of Zemax optimization and will have to be revisited when procured. The distribution of change in criterion by randomly varying the parameters within their limits using Monte Carlo simulation gives an estimate of the performance probability.

**Table 4.** Tolerance data listing for Model I.

sl.	parameters	surfaces	nominal	minimum	maximum	units
1	Test Wavelength	–	1000	–	–	Å
2	Radius of Curvature	OAP mirror	792	–1	1	mm
3	Sagittal radius of Curvature	Grating	396	–1	1	mm
4	Decenter	All surfaces	–	–0.5	0.5	mm
5	Tilt	All surfaces	–	–0.5	–0.5	deg
6	Conic Constant	All surfaces	–	–0.02	0.02	–

**Table 5.** Tolerance data listing for Model II.

sl.	parameters	surfaces	nominal	minimum	maximum	units
1	Test Wavelength	–	1000	–	–	Å
2	Radius of curvature	OAP mirror	792	–1	1	mm
3	Radius of curvature	Diffraction grating	189	–1	1	mm
4	Decenter (Y only)	All surfaces	–	–0.2	0.2	mm
5	Tilt (X only)	All surfaces	–	–0.5	0.5	Deg
6	Conic Constant	OAP mirror	–1	–0.02	0.02	–
7	Conic Constant	Grating surface	0	–0.02	0.02	–

## 6. Conclusions and future plans

Our goal is to develop a small payload to study the diffuse FUV radiation field involving university students. This work is the first part in that effort: to design the optics necessary to achieve our science goals. We have found that a compact two bounce system would fit well into a small satellite. Adding a folding mirror serves to shrink the entire package further but at the cost of sensitivity. The effective area in the case of Model I is about 254 cm<sup>2</sup> yielding a sensitivity to diffuse sources of close to 1 photon cm<sup>-2</sup> s<sup>-1</sup> sr<sup>-1</sup> Å<sup>-1</sup> in a 1000 second observation in the center of the slit. The actual performance will be somewhat worse because of scattering from geocoronal Ly $\alpha$  but it is clear that we will easily be able to detect the diffuse radiation field.

We are now working with another group of students to design a mechanical structure for the optics which will fit into a small satellite bus, corresponding to dimensions seen in other ISRO small satellite proposals. We expect to have an engineering model completed by the end of 2009 after which we will explore further options to obtain the optics and the detectors for this mission. We note that the actual mission constraints are very loose and we can fly on either a low Earth mission or in a geostationary mission.

This approach has proven to be fruitful both in terms of the science goals and in terms of involving students in real-world science and engineering projects and we hope that we will be able to bring this to the natural conclusion of a space flight.

## References

- Murthy, J., 2009, *Ap&SS*, 320, 21  
Murthy, J. & Sahnou, D. J., 2004, *ApJ*, 615, 315  
Murthy, J., Hall, D., Earl, M., Henry, R. C. & Holberg, J. B. 1999, *ApJ*, 522, 904  
Wilkinson, E., Green, J. C., Osterman, S. N, Brownsberger, K. R., & Sahnou, D. J., 1998 *Proc. SPIE*, 3356, 18